ELECTROCHEMISTRY

Active sites of nitrogen-doped carbon materials for oxygen reduction reaction clarified using model catalysts

Donghui Guo,[1] Riku Shibuya,[2] Chisato Akiba,[2] Shunsuke Saji,[2] Takahiro Kondo,[1]* Junji Nakamura[1]*

Nitrogen (N)–doped carbon materials exhibit high electrocatalytic activity for the oxygen reduction reaction (ORR), which is essential for several renewable energy systems. However, the ORR active site (or sites) is unclear, which retards further developments of high-performance catalysts. Here, we characterized the ORR active site by using newly designed graphite (highly oriented pyrolitic graphite) model catalysts with well-defined π conjugation and well-controlled doping of N species. The ORR active site is created by pyridinic N. Carbon dioxide adsorption experiments indicated that pyridinic N also creates Lewis basic sites. The specific activities per pyridinic N in the HOPG model catalysts are comparable with those of N-doped graphene powder catalysts. Thus, the ORR active sites in N-doped carbon materials are carbon atoms with Lewis basicity next to pyridinic N.

The oxygen reduction reaction (ORR) is a key reaction for fuel cells and other renewable energy technologies such as metal-air batteries and dye-sensitized solar cells. Nitrogen-doped carbon materials as non-metal catalysts exhibit high electrocatalytic activity for the ORR (1, 2) and high durability, even under acidic conditions (3). Nitrogen-doped carbon materials are thus among the most promising candidates as alternatives to high-cost Pt catalysts for fuel cell applications. To be developed as high-performance catalysts, they should be engineered to contain a high concentration of active sites without inactive components. Hence, it is imperative to identify the active sites of nitrogen-doped carbon materials for the ORR, albeit still under debate. Currently, the debate focuses on whether the active sites are created by pyridinic N (pyri-N, N bonded to two carbon atoms) or graphitic N (grap-N, N bonded to three carbon atoms, also called substituted N or quaternary N) (4–13).

The controversy can be ascribed to two reasons. One is the mixing of different types of nitrogen species in the carbon materials, which is inevitable in the doping processes (e.g., by annealing under NH_3 atmosphere). The other lies in the inhomogeneities associated with the morphology and the graphitization level of the evaluated samples, which leads to inhomogeneous sizes of the π-conjugated system. Indeed, the size of nitrogen-doped graphene quantum dots has been reported to affect the ORR performance (14). Thus, it is difficult to determine which type of nitrogen creates the active site for the ORR by comparing samples subjected to treatment or pyrolysis at different temperatures because the size of the π-conjugated system is also dependent on the annealing temperature.

To determine the active site conclusively, we develop four types of model catalysts with well-defined π conjugation based on highly oriented pyrolytic graphite (HOPG): (i) pyridinic N–dominated HOPG (pyri-HOPG); (ii) graphitic N–dominated HOPG (grap-HOPG), and for comparison, (iii) edges patterned on the surface without N (edge-HOPG); and (iv) clean-HOPG (see supplementary methods and fig. S1). The active sites and adsorption properties of the nitrogen-doped carbon surfaces are examined by ORR, post-ORR x-ray photoelectron spectroscopy (XPS), and CO_2 temperature programmed desorption (TPD) measurements.

Of the four types of prepared HOPG model catalysts, preparation of the pyridinic N–dominated HOPG model catalyst is the most challenging because pyridinic N atoms are preferentially located at the edges of graphite. We thus designed an edge-patterned surface by Ar^+ etching through a mask. Figure 1 (A to D) shows surface morphological characterization of a typical edge-patterned model catalyst. The ordered uniform rectangular groove structures were distributed over the surface in a wide range. The atomic force microscopy (AFM) image presented in Fig. 1B shows dark regions corresponding to the grooves etched through the slits of the mask by ion beam and bright regions that correspond to nonetched surfaces. The surface of the bright region is intact and is basically flat. The profile of the blue line in Fig. 1B shows that the depth of the grooves is about 1200 ± 80 nm for this sample (Fig. 1D), which could be varied from about 100 nm to more than 2 μm by manipulating the etching energy and duration.

Figure 1E shows XPS N 1s spectra for clean-HOPG, edge-HOPG, grap-HOPG, and pyri-HOPG (C 1s and survey spectra are shown in fig. S2). The nondoped samples (clean-HOPG and edge-HOPG)

[1]Faculty of Pure and Applied Sciences, University of Tsukuba, 1-1-1 Tennodai, Tsukuba, Ibaraki 305-8573, Japan. [2]Graduate School of Pure and Applied Sciences, University of Tsukuba, 1-1-1 Tennodai, Tsukuba, Ibaraki 305-8573, Japan.
*Corresponding author. E-mail: takahiro@ims.tsukuba.ac.jp (T.K.); nakamura@ims.tsukuba.ac.jp (J.N.)

Table 1. Comparison of specific activity per pyridinic N of HOPG model catalysts (in Fig. 2) and N-GNS powder catalysts (in Fig. 4).

Sample	Nitrogen concentration (at. %)*	Pyridinic N concentration (at. %)*	$\|j\|$ at 0.5 V (mA cm^{-2})†	Specific activity per pyridinic N at 0.5 V (e$^-$ s^{-1} pyri-N^{-1})‡
Model HOPG-4	0.60	0.57	0.00041	0.12
Model HOPG-5	4.9	2.2	0.00090	0.066
Model HOPG-6	5.5	3.1	0.0016	0.082
Model HOPG-7	13	3.9	0.0026	0.11
Model HOPG-8	11	6.5	0.0055	0.14
N-GNS-1	1.7	0.72	0.085	0.07
N-GNS-2	2.4	1.9	0.37	0.11
N-GNS-3	8.1	6.3	1.4	0.13

*Nitrogen concentration evaluated by XPS.   †ORR current density obtained from current divided by geometric area of electrode surface.   ‡Activity derived from ORR current density ($\|j\|$), i.e., number of electrons converted by oxygen reduction per pyridinic N per second (e$^-$ s^{-1} pyri-N), as follows:

$$\text{Activity per pyridinic N} = \frac{\text{number of electrons per sec per cm}^2 \text{of electrode surface}}{\text{number of pyridinic N per cm}^2 \text{ of electrode surface}}$$

are indeed free of N, whereas N 1s peaks are observed for *grap*-HOPG and *pyri*-HOPG. The N concentrations of *grap*-HOPG and *pyri*-HOPG are 0.73 atomic % (82% for grap-N and 5% for pyri-N) and 0.60 atomic % (95% for pyri-N and 5% for grap-N), respectively, as estimated by the analysis of the peak areas for each element (N, C) by considering the atomic sensitivity of XPS. The N 1s spectra were analyzed by least-squares fitting analysis, which includes the components of pyridinic N (398.5 eV), graphitic N (401.1 eV), pyrrolic N (400.1 eV), and oxidic N (403.2 eV) (*15–18*).

The catalytic performance was measured by cyclic voltammetry (CV) in acidic electrolyte (0.1 M H_2SO_4) (electrode preparation is shown in fig. S3).

Figure 1F shows the ORR curves obtained under oxygen-saturated conditions with the subtraction of data under nitrogen-saturated conditions as the background, in which the currents are divided by the geometric surface areas of electrodes (the same as the exposed catalyst surface areas) as described in the experimental method of the supplementary materials. Figure 1F shows that the *pyri*-HOPG model catalyst displays high activity at high voltages, compared to the very low ORR activities of the N-free model catalysts. The *pyri*-HOPG sample with lower N concentration (N: 0.60 at. %) is much more active than the *grap*-HOPG sample with higher N concentration (N: 0.73 at. %). Since the *pyri*-HOPG sample is nearly

free of graphitic N, the ORR results indicate that pyridinic N rather than graphitic N reduces the ORR overpotential and creates the active site. The activity of the *grap*-HOPG sample could also be ascribed to the presence of pyridinic N as a minor component (0.04 at. %).

The dependence of the ORR activity of the catalyst on the concentration of pyridinic N was investigated and is presented in Fig. 2. Patterned HOPG model catalysts with higher nitrogen concentrations (*edge-N⁺*-HOPG) were prepared by N^+ ion beam etching through a Ni mask, which contain mixtures of different types of nitrogen (fig. S4 for N 1s and fig. S5 for survey and C 1s spectra). The ORR activities differed because of the different nitrogen-doping conditions (Fig. 2A). The current densities at a specific potential [potential versus reversible hydrogen electrode (RHE)] for each ORR were extracted and plotted versus the corresponding concentrations of pyridinic N and graphitic N. Figure 2B illustrates the linear relationship between the current densities and concentration of pyridinic N at each investigated potential, independent of the preparation method, indicating that the ORR activity is determined solely by the pyridinic N concentration. This linear dependence also suggests that the inhomogeneities in the graphitization and size of the π-conjugation system in the samples were overcome successfully in the HOPG model catalysts by applying the same annealing temperature of 973 K. In contrast, there is no correlation between the current density and the concentration of graphitic N (fig. S6). As a result, the onset potential (potential versus RHE at current density of 1 μA cm⁻²) increases with increasing concentration of pyridinic N (Fig. 2C).

We further investigated the intermediates of the ORR by ex situ post-ORR XPS measurements of the HOPG model, which reflects the steady-state surface of the N-HOPG model catalyst under ORR and provides mechanistic information about the active sites. Figure 3A illustrates a significant change in the N 1s peak (fig. S7 for C 1s) after the ORR half-cell measurement in acidic conditions, in which the concentration of pyridinic N (398.5 eV) decreased from 54 to 38%, and the concentration of the component corresponding to the 400.1 eV peak (either pyrrolic N or pyridonic N) increased from 11 to 29%, whereas the sum of the pyridinic N and pyrrolic/pyridonic N components remained largely constant (from 65 to 67%). By contrast, an N-HOPG sample after immersion in 0.1 M H_2SO_4 solution without the ORR scanning exhibited a negligible change in N 1s spectrum (fig. S8). The difference in the composition of nitrogen species before and after the ORR suggests that the carbon atoms next to pyridinic N react with OH species with consequent transformation of the pyridinic N to pyridonic N, as shown in Fig. 3B, suggesting that the active sites are the carbon atoms next to the pyridinic N rather than pyridinic N themselves.

Furthermore, we experimentally evaluated the relationship between the basicity and the activity of the HOPG model catalysts. Recently reported density functional theoretical (DFT) calculations
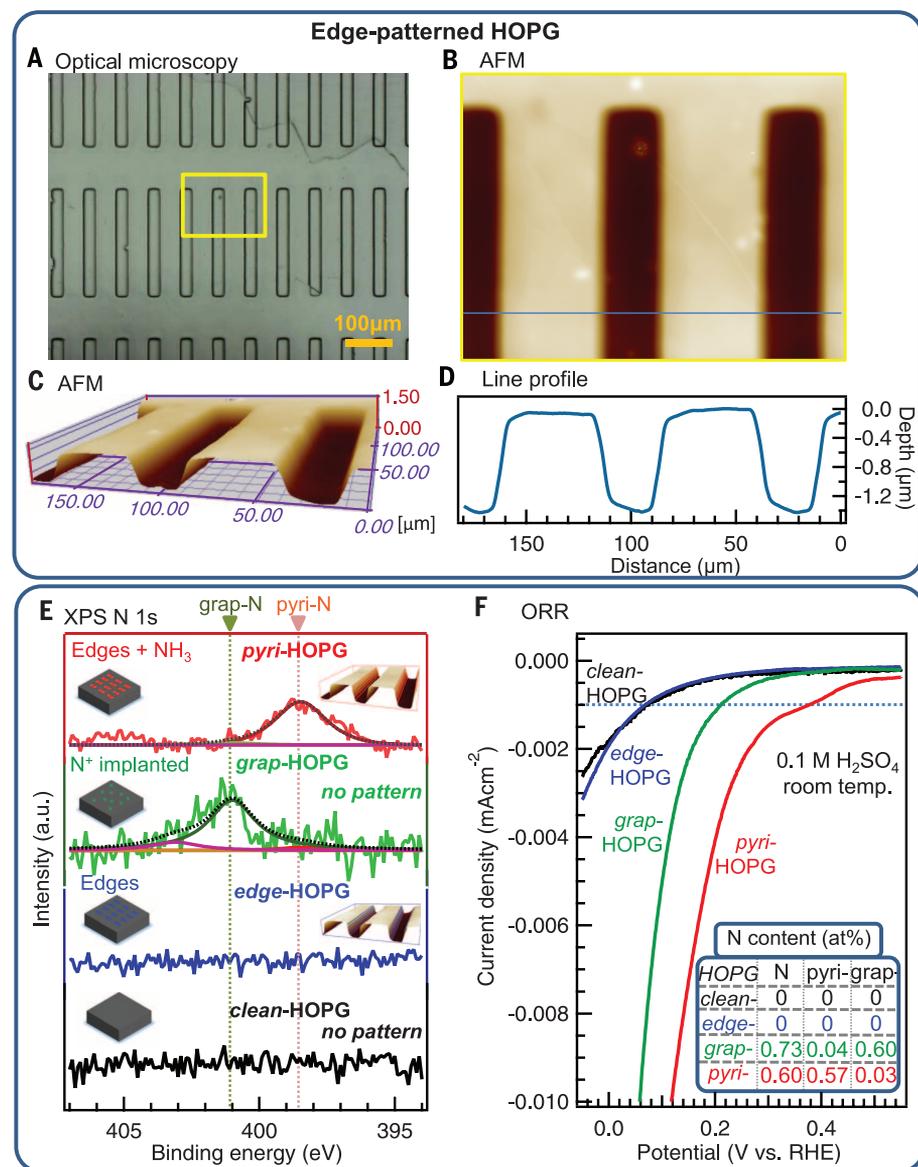

Fig. 1. Structural and elemental characterization of four types of N-HOPG model catalysts and their ORR performance. (**A**) Optical image of patterned *edge-N⁺*-HOPG. (**B**) The AFM image obtained for the region indicated by the yellow rectangle in (A). (**C**) Three-dimensional representation of (B). (**D**) Line profile of the AFM image obtained along the blue line in (B). (**E**) N 1s XPS spectra of model catalysts. (**F**) ORR results for model catalysts corresponding to (E). Nitrogen contents of the model catalysts are shown as the inset in (F).

suggested that carbon nanostructures containing pyridinic N possess Lewis basicity (19). Based on local scanning tunneling microscopy/spectroscopy (STM-STS) measurements combined with DFT calculations, it has also been reported that carbon atoms adjacent to pyridinic N possess a localized density of states in the occupied region near the Fermi level (20). This suggests that the carbon atoms can behave as Lewis bases owing to the possibility of electron pair donation. We thus examined the adsorption of CO_2 as a probe of the Lewis base site. Figure 3C shows the profiles for TPD of CO_2 from the HOPG model catalysts on which CO_2 was adsorbed at room temperature (fig. S9 shows N 1s XPS spectra). It is found that

acidic CO_2 molecule is adsorbed only on the ORR-active *pyri*-HOPG catalyst, which proves that the Lewis basic site is created by pyridinic N on the HOPG surface. It is generally known that oxygen molecules can be adsorbed on Lewis base sites (21). Because O_2 adsorption is the initial step of the ORR, the Lewis base site created by pyridinic N is thus suggested to be the active site for ORR.

To compare the HOPG model catalysts with powder catalysts, we prepared nitrogen-doped graphene nanosheets (N-GNS) and measured their ORR activities by the rotating disc method in 0.1 M H_2SO_4. Here, the N-GNS catalysts were prepared by the reaction of GNS with NH_3 at

973 K, which is the same temperature applied in the preparation of the HOPG model catalysts. Figure 4A shows the N 1s XPS profiles of the prepared N-GNS powder catalysts. The powder catalysts have high percentages of pyridinic N, and the pyridinic N concentration increases from N-GNS-1 (0.7 at. %) to N-GNS-2 (1.9 at. %) to N-GNS-3 (6.3 at. %), whereas the graphitic N concentrations are as low as 0.4 to 0.8 at. %. Figure 4B shows the ORR performances of the N-GNS powder catalysts, in which the currents are divided by the geometric electrode surface area (0.283 cm^2), with a loading amount of 0.02 mg. The ORR activity increases with increasing nitrogen concentration; e.g., the onset potential increases from
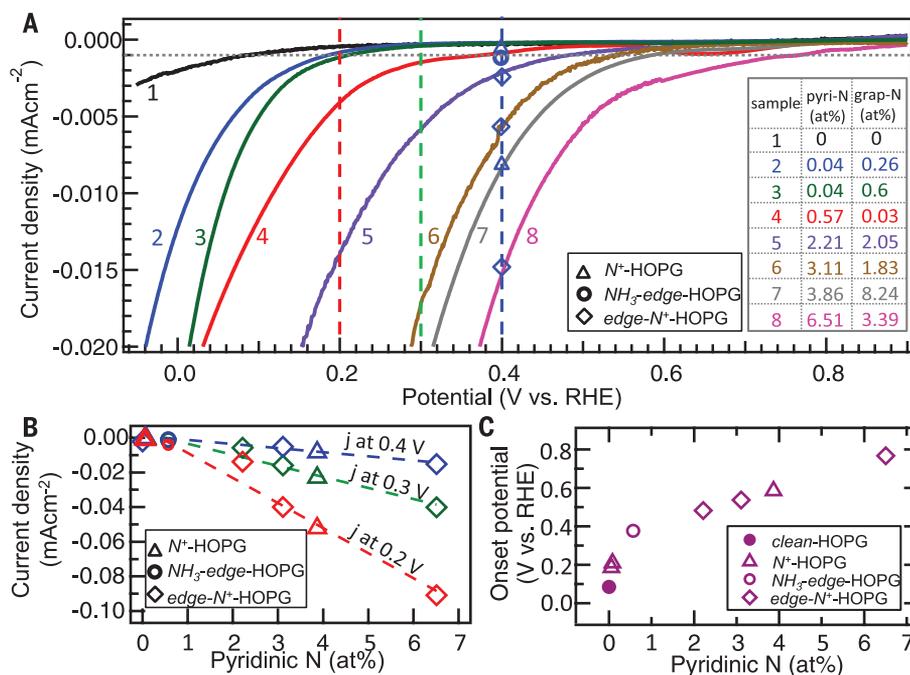

Fig. 2. Catalytic performance of N-HOPG model catalysts. (A) ORR results obtained for the model catalysts with different N concentrations. (B) Correlation between current densities of ORR at 0.2, 0.3, and 0.4 V versus RHE and the pyridinic N concentrations. (C) Correlation between onset potentials at 1 μA cm^{-2} and the pyridinic N concentrations. Different markers indicate different sample preparation methods. Nitrogen contents of the HOPG model catalysts are shown as the inset in (A).
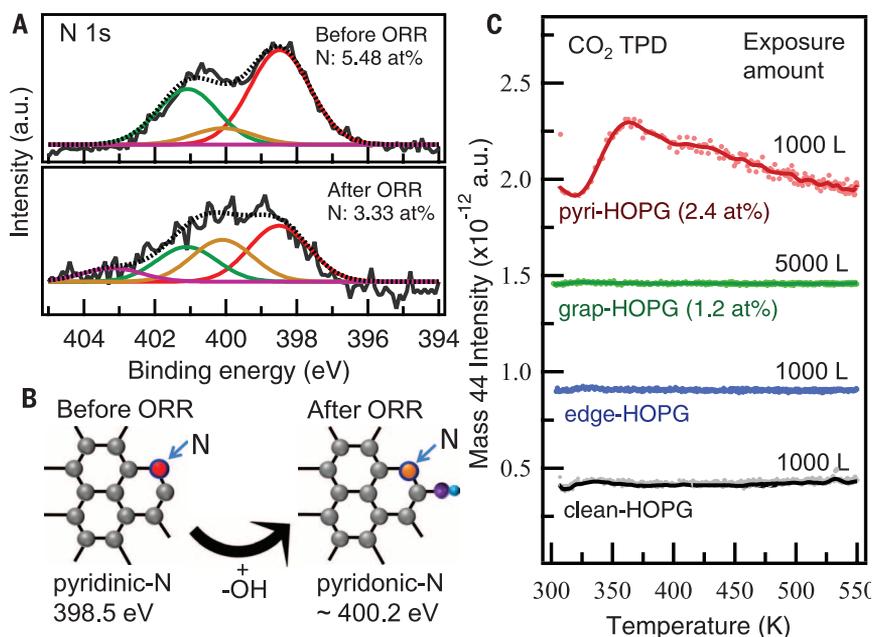
sample	pyri-N (at%)	grap-N (at%)
1	0	0
2	0.04	0.26
3	0.04	0.6
4	0.57	0.03
5	2.21	2.05
6	3.11	1.83
7	3.86	8.24
8	6.51	3.39

Fig. 3. Post-ORR XPS analysis and CO_2-TPD of the N-HOPG model catalysts. (A) N 1s XPS spectra of the N-HOPG model catalyst before and after ORR, respectively. (B) Schematic images of the formation of pyridonic N by the attachment of OH to the carbon atom next to pyridinic N. (C) CO_2-TPD results for the HOPG model catalysts.

Fig. 4. N 1s XPS spectra and ORR performance of N-GNS powder catalysts. (**A** and **B**) N 1s XPS spectra of N-GNS powder catalysts with different nitrogen concentrations and the corresponding ORR results. (**C**) Correlation between current densities of ORR at 0.5, 0.6, and 0.7 V versus RHE and pyridinic N concentrations.
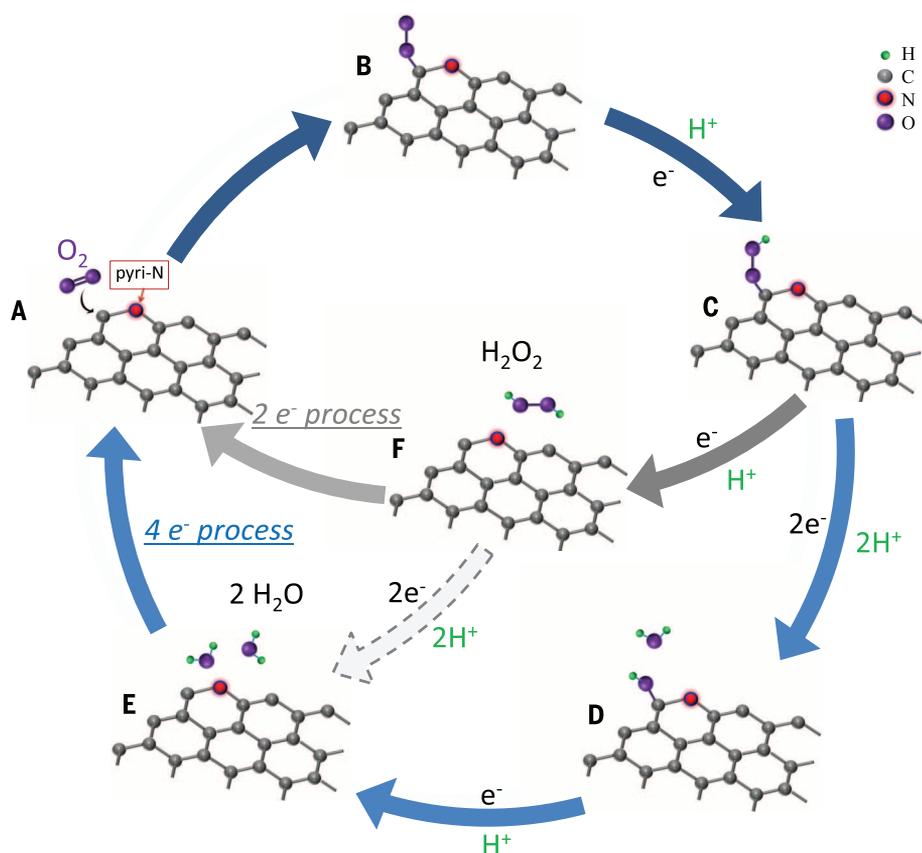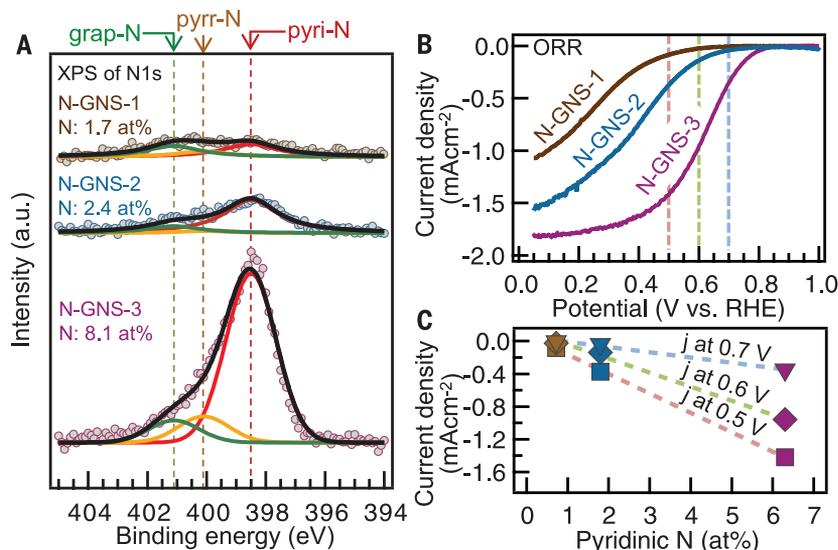

Fig. 5. Schematic pathway for oxygen reduction reaction on nitrogen-doped carbon materials.

0.77 V for N-GNS-1 to 0.91 V for N-GNS-3. The ORR activity was further examined in terms of the current densities at different potentials (0.5, 0.6, and 0.7 V versus RHE). The correlation between the ORR activities and the concentration of nitrogen species was examined for pyridinic N (Fig. 4C) and graphitic N (fig. S10). Linear relationships between the ORR activities at three different potentials and the concentration of py-ridinic N were obtained (Fig. 4C), consistent with the linear relationships for the HOPG model catalysts (Fig. 2). It is thus confirmed that pyridinic N creates the active site for ORR in the N-GNS powder catalysts.

We further compared the ORR specific activities of the N-HOPG model catalysts (in Fig. 2) and the N-GNS powder catalysts (in Fig. 4). The activities were evaluated by using the current densities at 0.5 V, at which the oxygen diffusion effect is not so pronounced for N-GNS and the current density is not so small for the N-HOPG model catalysts (comparison at 0.6 V is shown in table S1). As shown in Table 1, the current densities at 0.5 V (absolute value, $|j|$) for the N-HOPG model catalysts are approximately three orders of magnitude lower than those for the N-GNS powder catalysts, which can be attributed to the difference in the absolute number of active sites per 1 cm^2 of the geometric surface area of the electrodes. The N-HOPG model catalyst is simply a plate with a very low graphite surface area of about 0.1 cm^2, identical to the geometric electrode surface area. By contrast, the BET (Brunauer-Emmett-Teller) surface areas of the N-GNS catalysts on the electrode (0.283 cm^2) are about 80 cm^2 (see supplementary materials). As the pyridinic N creates the active site for ORR, we calculated the specific activities per pyridinic N for the model and powder catalysts and compared them by taking into account the BET surface area (400 $m^2\ g^{-1}$) for N-GNS (see supplementary methods for detailed calculation). The specific activities per pyridinic N are similar, at ~0.1 $e^-\ s^{-1}$ pyri-N^{-1} for both types of catalysts (0.07 to 0.14 $e^-\ s^{-1}$ pyri-N^{-1}). The agreement in the specific activity per pyridinic N indicates that, in general, the active sites of ORR for various kinds of nitrogen-doped carbon materials are created by pyridinic N.

Finally, we propose a possible mechanism for the ORR on nitrogen-doped carbon materials (Fig. 5). As the Lewis base site is created by pyridinic N, the oxygen molecule is first adsorbed at the carbon atom next to the pyridinic N followed by protonation of the adsorbed O_2. Two pathways are then possible: One is the four-electron mechanism taking place at a single site, and the other is the 2 + 2–electron mechanism, which does not always take place at a single site. In the four-electron mechanism, the other two protons attach to the two oxygen atoms, leading to breakage of the O-OH bond and formation of OH species ("D" in Fig. 5) as observed in post-ORR

XPS (Fig. 3). The additional proton then reacts with the adsorbed OH to form H_2O ("E" in Fig. 5). In the 2 + 2–electron pathway, H_2O_2 is formed by reaction of the adsorbed OOH species with another proton ("F" in Fig. 5), followed by readsorption of H_2O_2 and its reduction by two protons to generate H_2O. The OH species detected in the post-ORR XPS measurement may arise from the four-electron mechanism, but it is also possible that the OH species next to the pyridinic N may arise from the reaction with H_2O_2 in the 2 + 2–electron mechanism. In either pathway, the carbon atoms next to pyridinic N with Lewis basicity play an important role as the active sites at which oxygen molecules are adsorbed as the initial step of the ORR.

In summary, we have demonstrated that pyridinic N in nitrogen-doped graphitic carbons creates the active sites for ORR under acidic conditions, based on studies of HOPG model catalysts and N-GNS powder catalysts. Carbon atoms next to pyridinic N are suggested to be the active sites with Lewis basicity at which O_2 molecules are adsorbed as the initial step of the ORR.

REFERENCES AND NOTES

1. K. Gong, F. Du, Z. Xia, M. Durstock, L. Dai, *Science* **323**, 760–764 (2009).
2. L. Dai, Y. Xue, L. Qu, H.-J. Choi, J.-B. Baek, *Chem. Rev.* **115**, 4823–4892 (2015).
3. J. Shui, M. Wang, F. Du, L. Dai, *Sci. Adv.* **1**, e1400129 (2015).
4. H.-W. Liang, X. Zhuang, S. Brüller, X. Feng, K. Müllen, *Nat. Commun.* **5**, 4973 (2014).
5. L. Qu, Y. Liu, J.-B. Baek, L. Dai, *ACS Nano* **4**, 1321–1326 (2010).
6. C. V. Rao, C. R. Cabrera, Y. Ishikawa, *J. Phys. Chem. Lett.* **1**, 2622–2627 (2010).
7. T. Xing et al., *ACS Nano* **8**, 6856–6862 (2014).
8. R. Liu, D. Wu, X. Feng, K. Müllen, *Angew. Chem.* **49**, 2565–2569 (2010).
9. H. Niwa et al., *J. Power Sources* **187**, 93–97 (2009).
10. H. Kim, K. Lee, S. I. Woo, Y. Jung, *Phys. Chem. Chem. Phys.* **13**, 17505–17510 (2011).
11. N. P. Subramanian et al., *J. Power Sources* **188**, 38–44 (2009).
12. L. Lai et al., *Energy Environ. Sci.* **5**, 7936–7942 (2012).
13. W. Ding et al., *Angew. Chem. Int. Ed.* **52**, 11755–11759 (2013).
14. Q. Li, S. Zhang, L. Dai, L. S. Li, *J. Am. Chem. Soc.* **134**, 18932–18935 (2012).
15. S. Maldonado, S. Morin, K. J. Stevenson, *Carbon* **44**, 1429–1437 (2006).
16. E. Raymundo-Piñero et al., *Carbon* **40**, 597–608 (2002).
17. J. R. Pels, F. Kapteijn, J. A. Moulijn, Q. Zhu, K. M. Thomas, *Carbon* **33**, 1641–1653 (1995).
18. I. Kusunoki et al., *Surf. Sci.* **492**, 315–328 (2001).
19. B. Li, X. Sun, D. Su, *Phys. Chem. Chem. Phys.* **17**, 6691–6694 (2015).
20. T. Kondo et al., *Phys. Rev. B* **86**, 035436 (2012).
21. H. Metiu, S. Chrétien, Z. Hu, B. Li, X. Sun, *J. Phys. Chem. C* **116**, 10439–10450 (2012).

MOLECULAR FRAMEWORKS

Weaving of organic threads into a crystalline covalent organic framework

Yuzhong Liu,[1]* Yanhang Ma,[2]* Yingbo Zhao,[1]* Xixi Sun,[1] Felipe Gándara,[3] Hiroyasu Furukawa,[1] Zheng Liu,[4] Hanyu Zhu,[5] Chenhui Zhu,[6] Kazutomo Suenaga,[4] Peter Oleynikov,[2] Ahmad S. Alshammari,[7] Xiang Zhang,[5,8] Osamu Terasaki,[2,9]† Omar M. Yaghi[1,7]†

A three-dimensional covalent organic framework (COF-505) constructed from helical organic threads, designed to be mutually weaving at regular intervals, has been synthesized by imine condensation reactions of aldehyde functionalized copper(I)-bisphenanthroline tetrafluoroborate, $Cu(PDB)_2(BF_4)$, and benzidine (BZ). The copper centers are topologically independent of the weaving within the COF structure and serve as templates for bringing the threads into a woven pattern rather than the more commonly observed parallel arrangement. The copper(I) ions can be reversibly removed and added without loss of the COF structure, for which a tenfold increase in elasticity accompanies its demetalation. The threads in COF-505 have many degrees of freedom for enormous deviations to take place between them, throughout the material, without undoing the weaving of the overall structure.

Weaving, the mutual interlacing of long threads, is one of the oldest and most enduring methods of making fabric, but this important design concept has yet to be emulated in extended chemical structures. Learning how to link molecular building units by strong bonds through reticular synthesis (*1*) into weaving forms would be a boon to making materials with exceptional mechanical properties and dynamics. To successfully design weaving of chains into two- and three-dimensional (2D and 3D) chemical structures (Fig. 1, A and B), long threads of covalently linked molecules (i.e., 1D units) must be able to cross at regular intervals. It would also be desirable if such crossings serve as points of registry, so that the threads can have many degrees of freedom to move away from and back to such points without collapsing the overall structure. Structures have been made by weaving metal-organic chains (*2*), but designing well-defined materials and assembling their structures by weaving is challenging, and weaving in crystalline inorganic or covalent organic extended structures is undeveloped.

We report on a general strategy and its implementation for the designed synthesis of a woven material [covalent organic framework-505 (COF-505)]. This COF has helical organic threads interlacing to make a weaving crystal structure with the basic topology of Fig. 1B, and we show that this material has an unusual behavior in elasticity. Although terms such as interweaving (*3*), polycatenated (*2*), and interpenetrating (*4–6*) have been used to describe interlocking of 2D and 3D extended objects (Fig. 1, C and D), most commonly found in MOFs, we reserve the term "weaving" to describe exclusively the interlacing of 1D units to make 2D and 3D structures (Fig. 1, A and B). Weaving differs from the commonly observed interpenetrating and polycatenated frameworks because the latter are topologically interlocking

[1]Department of Chemistry, University of California, Berkeley, Materials Sciences Division, Lawrence Berkeley National Laboratory, and Kavli Energy NanoSciences Institute, Berkeley, CA 94720, USA. [2]Department of Materials and Environmental Chemistry, Stockholm University, SE-10691 Stockholm, Sweden. [3]Department of New Architectures in Materials Chemistry, Materials Science Institute of Madrid, Consejo Superior de Investigaciones Científicas, Madrid 28049, Spain. [4]Nanomaterials Research Institute, National Institute of Advanced Industrial Science and Technology (AIST), Tsukuba 305-8565, Japan. [5]NSF Nanoscale Science and Engineering Center (NSEC), University of California at Berkeley, 3112 Etcheverry Hall, Berkeley, CA 94720, USA. [6]Advanced Light Source, Lawrence Berkeley National Laboratory, Berkeley, CA 94720, USA. [7]King Abdulaziz City of Science and Technology, Post Office Box 6086, Riyadh 11442, Saudi Arabia. [8]Material Sciences Division, Lawrence Berkeley National Laboratory, 1 Cyclotron Road, Berkeley, CA 94720, USA. [9]School of Physical Science and Technology, ShanghaiTech University, Shanghai 201210, China.
*These authors contributed equally to this work. †Corresponding author. E-mail: terasaki@mmk.su.se (O.T.); yaghi@berkeley.edu (O.M.Y.)